Journal of Medicinal Chemistry

pubs.acs.org/jmc

Article

Cyclodextrin-Activated Porphyrin Photosensitization for Boosting Self-Cleavable Drug Release

Mian Tang, Yanqiu Song, Yi-Lin Lu, Ying-Ming Zhang,* Zhilin Yu, Xiufang Xu, and Yu Liu*

Cite This: J. Med. Chem. 2022, 65, 6764−6774

Read Online

ACCESS | Metrics & More | Article Recommendations | Supporting Information

ABSTRACT: Supramolecular prodrugs that combine the merits of stimuli-responsiveness and targeting ability in a controllable manner have shown appealing prospects in disease diagnostics and therapeutics. Herein, we report that a new theranostic agent with the host−guest-binding-activated photosensitization has been fabricated by a binary supramolecular assembly consisting of the permethyl-β-cyclodextrin-grafted hyaluronic acid and a combretastatin A-4-appended porphyrin derivative. Illuminated by a red-light source, the production efficiency of singlet oxygen ($^1O_2$) pronouncedly increases by ∼60-fold once the porphyrin core is encapsulated by cyclodextrins. Consequently, the cell-selective fluorescence emission is dramatically enhanced, the microtubule-targeted drug is rapidly and completely released, and the $^1O_2$-involved combinational treatment is simultaneously achieved both in vitro and in vivo. To be envisaged, this complexation-boosted light-activatable photosensitizing prodrug delivery system with improved photophysical performance and remarkable phototheranostic outcomes will make a significant contribution to the creation of more advanced stimulus-based biomaterials.

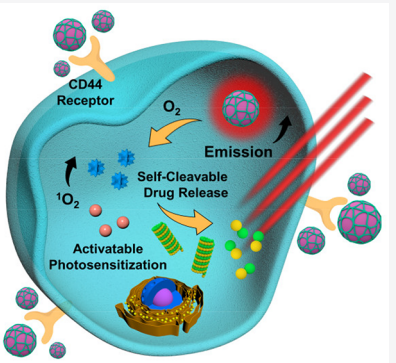

INTRODUCTION

A combination of the innate advantages of supramolecular chemistry and medical science has expedited the emergence of supramolecular prodrugs,[1−5] by which bioactive molecules can be endowed with desired solubility, targeting, and stimuli-responsive abilities in a noncovalent and controllable manner.[6−10] Compared to those classic prodrugs that merely rely on the covalent modification of active drugs, supramolecular prodrugs derived from multiple noncovalent interactions can be classified as an important branch of modern nanomedicines and have provided an emerging paradigm for combating many life-threatening diseases.[11−14] Along with the substantial development of supramolecular prodrugs, in particular, light-activatable theranostic nanosystems have served as one of the most promising candidates, owing to their spatiotemporal controllability and noninvasive nature of light input, as well as the fact that light-mediated activation can trigger a cascade of photochemical reactions and exert a strong influence on the emergence of more advanced therapeutic methods, such as photodynamic therapy, photothermal therapy, photoacoustic imaging, and so on.[15−23] It is of great significance to manipulate the photophysical properties of optically active agents at different molecular levels and improve the efficiency of current photoderived treatments for biotechnological innovation.

As for the design of light-activatable prodrugs, host−guest complexation with some well-crafted macrocyclic receptors, such as cyclodextrin, calixarenes, cucurbiturils, and pillararenes, has been drawn into the limelight and believed as a simple yet feasible way of conferring smart chemistry to conventional chemotherapeutic agents that lack environmentally responsive characteristics.[24−28] By leveraging the host−guest interactions, one can efficiently regulate the aggregate states, photoluminescence behaviors, and pharmacokinetic properties of a given optically active agent, which have critical relevance to the phototheranostic outcomes of a single self-assembled entity.[29−32] Diverse types of macrocyclic hosts have been proven to possess strikingly distinctive abilities in manipulating the excitation energy dissipation pathways of a given organic optical agent, thus allowing for creation of functional nanomaterials with great potential in biological imaging and disease treatments. The macrocycle-based host−guest-binding strategy has greatly expanded the research scope for supramolecular prodrugs and provided researchers with bountiful opportunities for stimulus-based biotransformation with easier construction and better therapeutic effects than parent species.[33,34]

Inspired by our ongoing interests concerning the fabrication of host−guest-binding-induced photoluminescent supramolecular assemblies, we herein demonstrate a novel light-activatable prodrug delivery platform by implementing the complexation-enhanced photosensitization for targeted cancer theranostics.

Received: January 19, 2022
Published: April 29, 2022

https://doi.org/10.1021/acs.jmedchem.2c00105
J. Med. Chem. 2022, 65, 6764−6774

Scheme 1. Illustration of TPP-CA4⊂HA-PMeCD Nanoparticles with Cyclodextrin-Boosted Porphyrin Photosensitization and Self-Photocleavable Drug Release

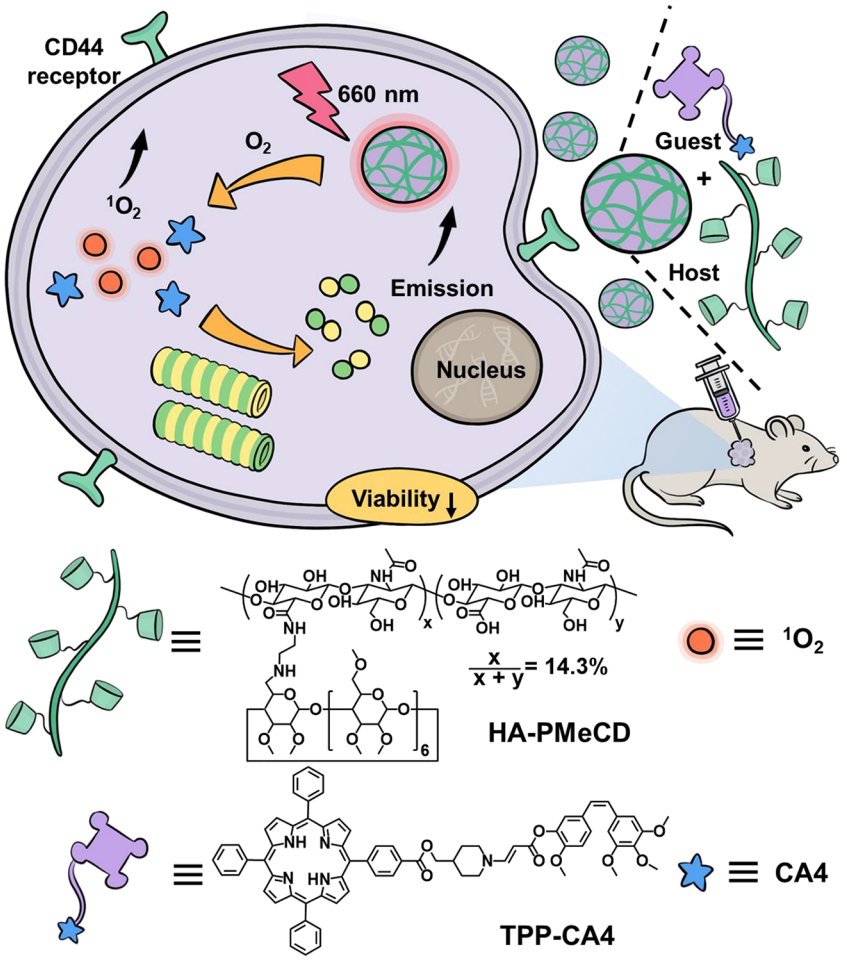

This binary supramolecular prodrug is composed of the permethyl-β-cyclodextrin-grafted hyaluronic acid (HA-PMeCD) and a 5-(4-carboxyphenyl)-10,15,20-triphenylporphyrin derivative (TPP-CA4) bearing combretastatin A-4 (CA4) and the singlet oxygen ($^1O_2$)-cleavable aminoacrylate group (Scheme 1). CA4 is a well-known tubulin binder that can inhibit tubulin polymerization and block the mitosis process of tumor cells.[35,36] Also, the inclusion complexation of the hydrophobic TPP-CA4 core with the hydrophilic HA-PMeCD shell can not only give rise to the formation of nanoparticulate assemblies for the internalization in cells but also endow them with the desired targeting ability via the specific receptor-mediated recognition on the cell surface.[37−39] Moreover, the encapsulation with PMeCD can protect the entire assembly from the unspecific attack with biomacromolecules.[40] Remarkably, the extensive host−guest complexation can dramatically enhance the fluorescence emission and facilitate $^1O_2$ transfer from the photosensitizing center to the aminoacrylate linker, further simulating the release of microtubule (MT)-targeted CA4 drug and strengthening the combinational effect.[41,42] This supramolecular prodrug delivery system based on cyclodextrin-activated porphyrin photosensitization may provide a promising approach to develop advanced nanomedicines for targeted bioimaging and combinational treatment.

RESULTS AND DISCUSSION

Synthesis and Host−Guest Complexation Characterization. The self-assembling process of TPP-CA4⊂HA-PMeCD assembly is depicted in Scheme 1. The compound characterization is shown in the Supporting Information (Figures S1−S4, Supporting Information). The prodrug TPP-CA4 is composed of tetraphenylporphyrin (TPP) and combretastatin A-4 (CA4) as photosensitizing and therapeutic agents, respectively, which are covalently connected with each other by the $^1O_2$-cleavable aminoacrylate group. In general, some highly efficient photosensitizers, such as core-modified porphyrins, should be utilized to efficiently cleave $^1O_2$-sensitive chemical bonds.[43,44] However, such molecular design can inevitably be subjected to time-consuming chemical synthesis and inadvertent photosensitizer activation. In our case, by using the commercially available monocarboxylic porphyrin, the prodrug TPP-CA4 could be easily obtained in only three steps. Next, the molecular binding mode and strength between PMeCD and the porphyrin skeleton were studied using the esterified porphyrin (TPP-$COOCH_3$) as a reference compound. The UV−vis absorbance of TPP-$COOCH_3$ steadily increased upon the addition of PMeCD, accompanied by the appearance of an isosbestic point at 424 nm (Figure 1a). After validation of the 1:2 complexation stoichiometry by Job's plot, the stepwise binding constants (K_1 and K_2) could be calculated as 1.86×10^4 and 2.34×10^3 M^{-1}, respectively (Figures 1b and

https://doi.org/10.1021/acs.jmedchem.2c00105
J. Med. Chem. 2022, 65, 6764−6774

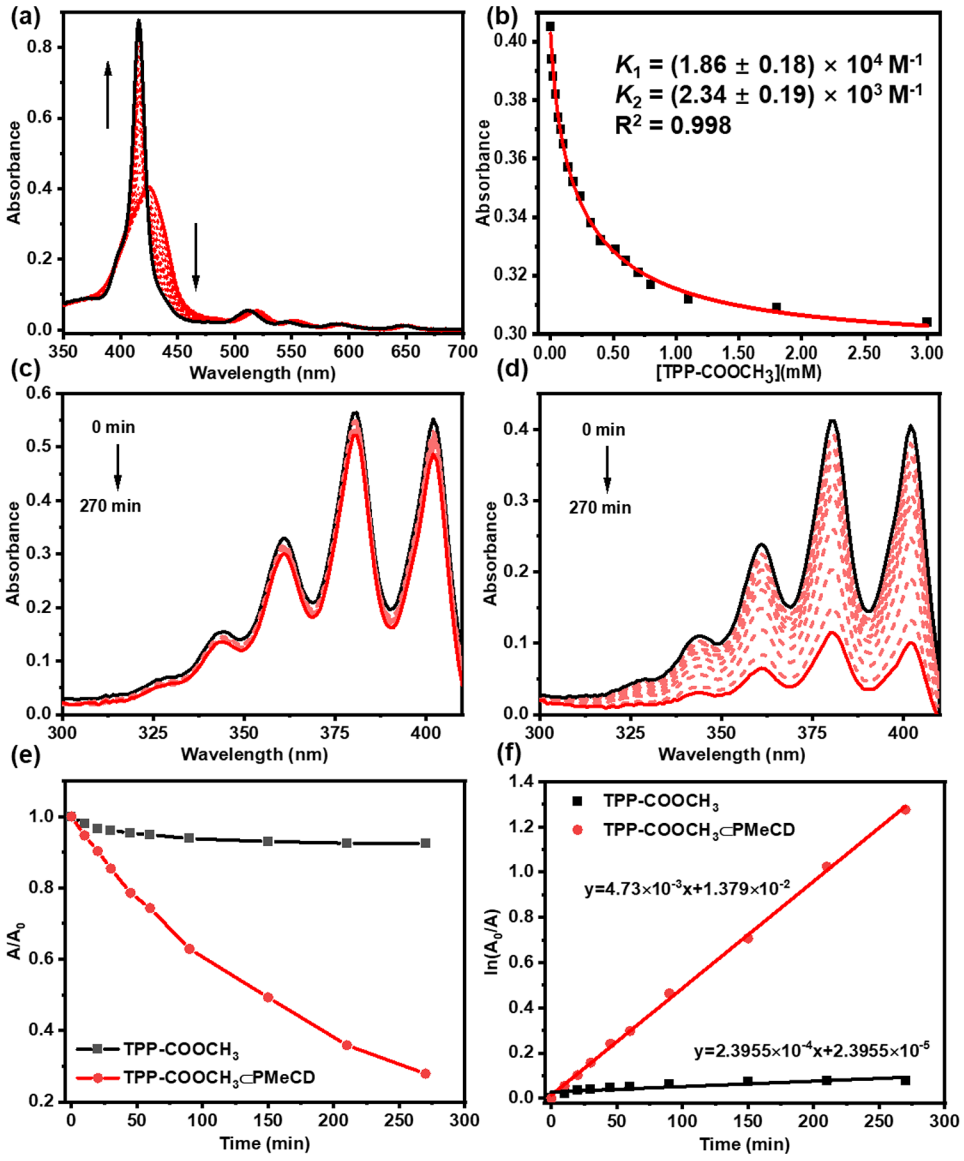

Figure 1. (a) UV−vis spectral changes of TPP-$COOCH_3$ upon addition of PMeCD ([TPP-$COOCH_3$] = 10.0 μM, [PMeCD] = 0−0.03 mM, 10% DMSO in PBS); (b) calculation of the K_S values by the nonlinear least-squares curve-fitting method; UV−vis spectra of ABDA in the presence of (c) TPP-$COOCH_3$ and (d) TPP-$COOCH_3$⊂PMeCD complex under 650 nm light irradiation. The decreased UV−vis absorbance indicates that ABDA was gradually consumed by the photochemically generated $^1O_2$. (e) Normalized UV−vis absorbance of ABDA at 380 nm after photodecomposition by $^1O_2$ upon light irradiation at 650 nm. (f) Decomposition rate of ABDA with TPP-$COOCH_3$ and TPP-$COOCH_3$⊂PMeCD complex. ([PMeCD] = 2[TPP-$COOCH_3$] = 20 μM, [ABDA] = 50 μM, 1% DMSO in PBS).

S5, Supporting Information). Meanwhile, the fluorescence emission intensity of porphyrin in the presence of PMeCD was 2-fold higher than that in the absence of PMeCD (Figure S6, Supporting Information).

Singlet Oxygen Generation and Photocleavable Drug Release Abilities. As discerned from Figure 1c−f, it is found that the $^1O_2$ quantum yields (ϕ_Δ) of TPP-$COOCH_3$ showed a sudden leap by a factor of 57.3 after complexation with PMeCD using 9,10-anthracenediyl-bis(methylene)-dimalonic acid (ABDA) as the $^1O_2$ indicator and methylene blue as the standard substance.[45,46] Benefiting from the complexation-boosted $^1O_2$ production, it is expected that the aminoacrylate linker could be efficiently photocleaved, thus leading to the rapid release of CA4 drug. To verify the complexation-induced $^1O_2$ production and concomitant drug release, high performance liquid chromatography (HPLC) was performed. As can be seen from Figure 2b, the drug release from TPP-CA4 slowly proceeded upon light irradiation at 650 nm for 5 h (retention time = 4.6 min). In stark contrast, with the assistance of PMeCD, the drug release process was clearly detected under light irradiation for only 5 min and CA4 was completely released in 15 min (Figure 2c). These results indicate that the noncovalent association of the porphyrin core with PMeCD can significantly promote $^1O_2$ production and accelerate the photooxidation process, resulting in the prompt and complete release of drug molecules.

Furthermore, the photostability of TPP-CA4 and TPP-CA4⊂PMeCD complex was also comparatively investigated by chromatography and spectroscopy. In our case, the photocleavage process of the TPP-CA4 prodrug can be monitored by the resonance peaks of aldehyde group in the NMR spectra (δ = 8.11 ppm in Figures S7 and S8, Supporting Information).

https://doi.org/10.1021/acs.jmedchem.2c00105
J. Med. Chem. 2022, 65, 6764−6774

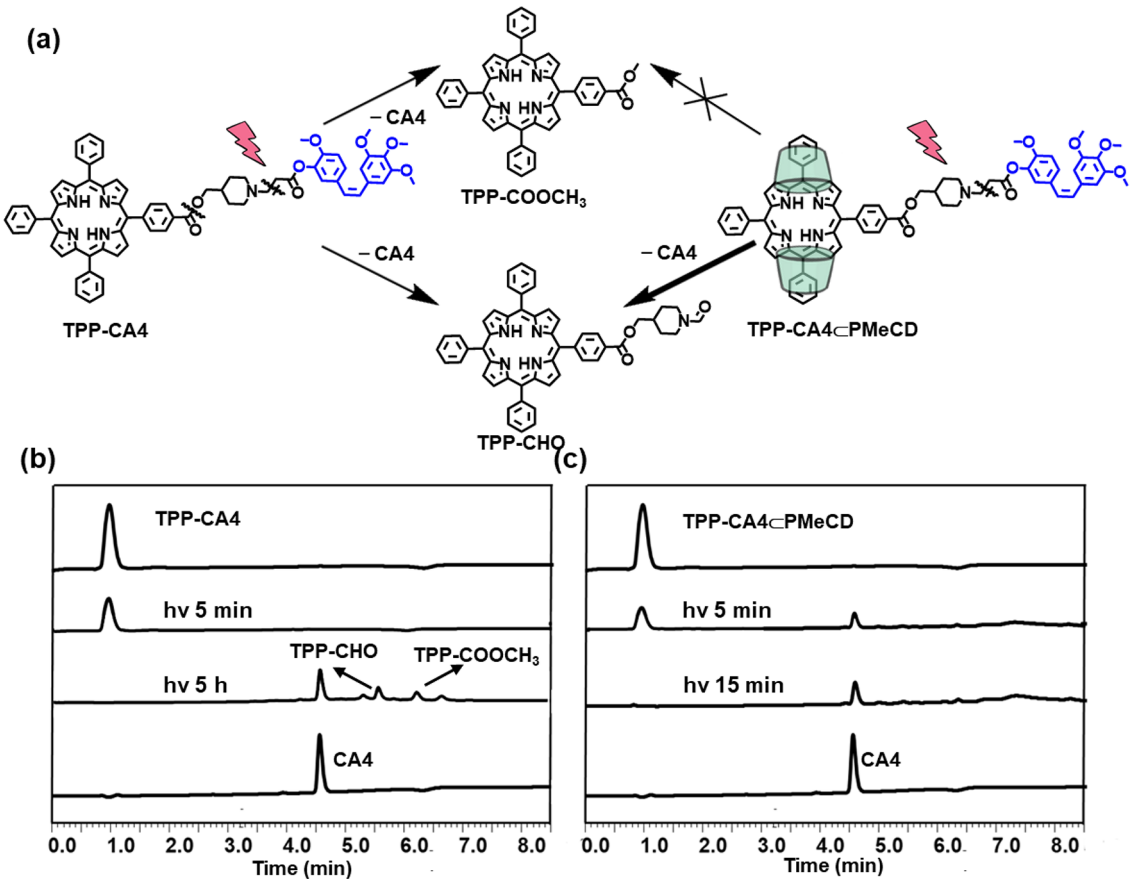

Figure 2. (a) Schematic representation of the PMeCD-boosted release of CA4. HPLC retention times of (b) TPP-CA4 and (c) TPP-CA4⊂PMeCD complexes versus different irradiation times ([TPP-CA4] = 10 μM and [PMeCD] = 20 μM). The detection wavelength in each trace was set as 254 nm.

Through the calculation of the integration area of olefinic protons, the photooxidation reaction could be completely achieved in 5 h (Table S1 and Figure S9, Supporting Information). It is shown that the integral area of olefinic proton (H_b) in TPP-CA4 gradually decreased, while the one of aldehyde proton (H_c) in the photooxidation product gradually increased, indicative of the photocleaved drug release under light irradiation. The emergence of released CA4 could also be conveniently monitored by thin-layer chromatography (R_f = 0.6 in Figure S10, Supporting Information). In addition, the spontaneous methyl easternization of TPP occurred in methanol, whereas no such phenomenon was observed in the presence of PMeCD (Figures 2a and S11, Supporting Information). Meanwhile, although the UV−vis absorbance intensity was basically unchanged, the photoluminescence properties were strikingly distinct before and after inclusion complexation with PMeCD. That is, the fluorescence emission intensity of TPP-CA4 alone slightly declined upon exposure to light irradiation for 1 h, whereas strong fluorescence enhancement was observed in the TPP-CA4⊂PMeCD complex under the same experimental conditions (Figure S12, Supporting Information). Apparently, such fluorescence enhancement would facilitate the fluorescence imaging and monitoring after the photoactivated drug release.

The mechanism behind these photophysical behaviors was substantiated by computational studies. By comparison of the orbital energies of CA4 and TPP-CHO, the photoinduced electron transfer pathway was not responsible for the fluorescence quenching (Figures S13 and S14, Supporting Information). In addition, no obvious change in intermolecular distance, dihedral angle, or binding energy was found upon complexation of PMeCD with TPP-CHO or TPP-CA4 (Figures 3a,b and S15, Table S2, Supporting Information), but the fluorescence emission became much stronger when the flexible substituents in TPP-CA4 were photocleaved (Figure S16, Supporting Information). These phenomena jointly demonstrate that unfavorable vibration or rotation of chemical bonds could be greatly suppressed after the drug release and thus result in the complexation-induced fluorescence enhancement. Undoubtedly, these complexation-improved photophysical performances would eventually facilitate the consequent bioimaging, cell damage, and even therapeutic outcomes in cancer treatment, as described below.

Binary Supramolecular Assembling Process. Subsequently, the molecular assembling behaviors between HACD and TPP-CA4 have been investigated. In our case, the degree of substitution of PMeCD units in HACD was 14.3%, which can maintain the balance of CD's encapsulation ability and HA's targeting ability toward malignant cells.[47−49] The simple mixing of TPP-CA4 with PMeCD gave uniform size distribution with an average hydrodynamic diameter of approximately 121 nm, accompanied by the palpable Tyndall effect in solution (Figure 3c and inset photo). Meanwhile, the ζ potential of the binary assembly was measured as −35.2 mV, which is attributed to the negative charges on the HA surface (Figure 3c, inset photo). Along with the observations in

https://doi.org/10.1021/acs.jmedchem.2c00105
J. Med. Chem. 2022, 65, 6764−6774

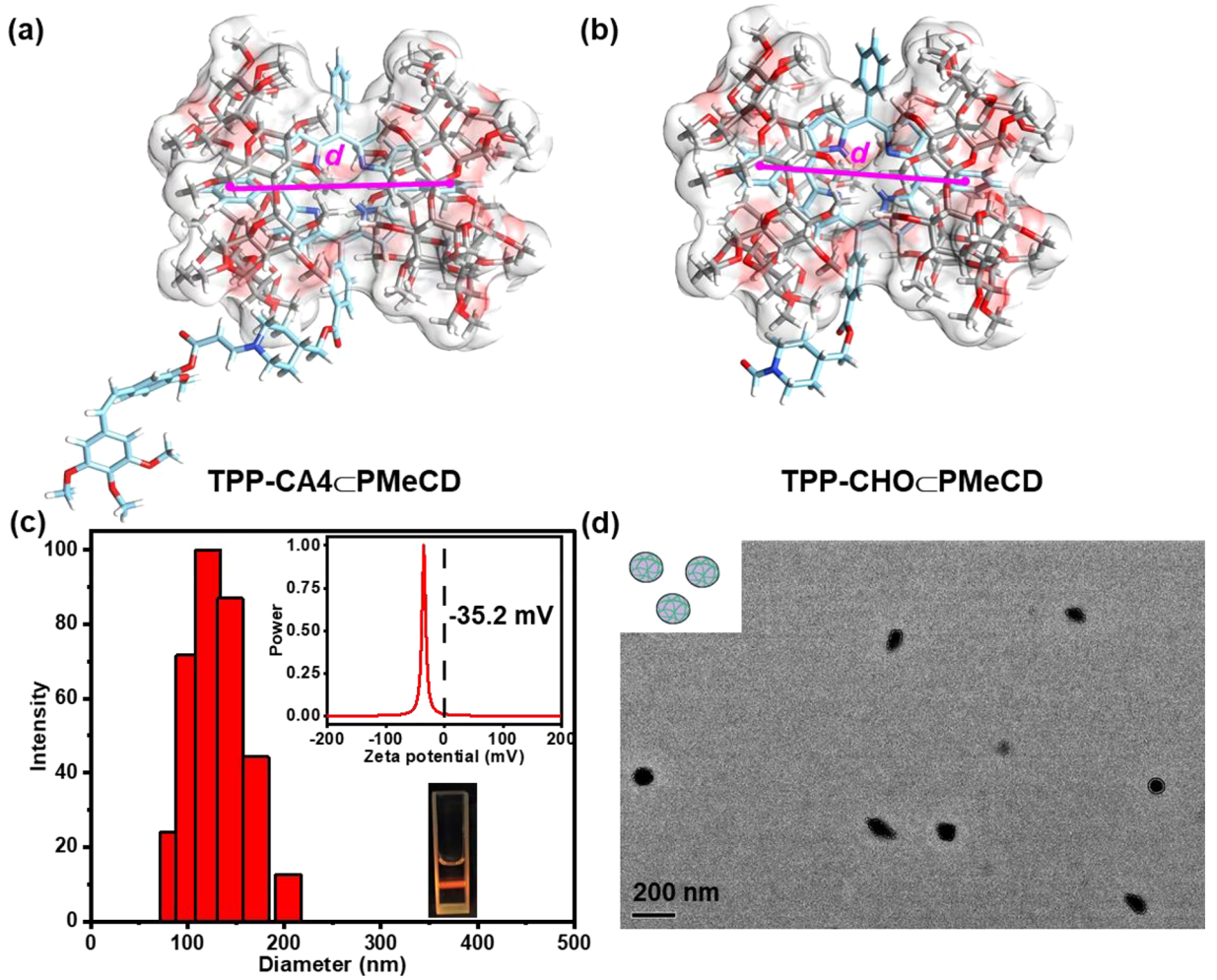

Figure 3. Intermolecular distances (d) between two adjacent PMeCD in (a) the TPP-CA4⊂PMeCD complex (d = 11.1 Å) and (b) TPP-CHO⊂PMeCD complex (d = 11.3 Å), where the pink point is the geometric center of each PMeCD. Average dihedral angle (φ) is between the planes of the phenyl ring and porphyrin core in the cavity of PMeCD. (c) Size distributions (inset: ζ potential and Tyndall effect) of the binary assembly in PBS ([TPP-CA4] = 10 μM, [HA-PMeCD] = 20 μM, pH 7.2); (d) TEM image of TPP-CA4⊂HA-PMeCD assembly.

aqueous solution, nanoparticulate aggregates with diameter of ∼100 nm could be readily observed in the transmission electron microscopic (TEM) image, mainly due to the extensive intermolecular cross-linkage of HA polymers by 1:2 TPP-CA4⊂PMeCD complexation (Figure 3d). These results jointly demonstrate the formation of biocompatible large-sized nanostructures by multivalent host−guest interactions, which would promote the receptor-mediated internalization by cancer cells.

Photoactivated Drug Release and Anticancer Activities in Vitro. Confocal laser scanning microscopy was further employed to investigate the complexation-induced cytoskeletal changes and photodynamic outcomes in the human lung adenocarcinoma (A549) cells and human renal epithelial (293T) cells. In the dark, the pristine MTs were uniformly dispersed as filaments around the nucleus when the cells were co-incubated with TPP-CA4 or TPP-CA4⊂HA-PMeCD complex (Figures S17 and S18, Supporting Information). In addition, relatively weak red fluorescence emission of TPP-CA4 was observed upon complexation with HA-PMeCD exclusively in the A549 cells, implying that the binary assembly could be easily internalized in cancer cells. Under light irradiation, normal MT morphology was still maintained in the control group but it was converted to the scattered dots in the TPP-CA4 group (Figure 4a-ii and Figure 4a-iii). Notably, in the case of the TPP-CA4⊂HA-PMeCD assembly, more cells could be observed with significant cytoskeletal changes, accompanied by the emergence of red fluorescence emission in A549 cells. Obviously, the released CA4 drug could seriously interfere with the tubulin growth along the MT backbone as a result of the $^1O_2$-sensitive self-photocleavage of aminoacrylate bond. In comparison, in the absence of HA receptors, no red fluorescence emission was observed and MTs were well-preserved in 293T cells (Figure 4b). Meanwhile, the $^1O_2$ generation ability was qualitatively explored in the selected cell line by using 6-carboxy-2′,7′-dichlorodihydrofluorescein diacetate (DCFH-DA) as the detecting probe. As shown in Figure S19 (Supporting Information), green fluorescence emission was shown in the TPP-CA4 group, but the emission turned much brighter in the group of TPP-CA4⊂HA-PMeCD assembly, indicative of the higher efficiency of $^1O_2$ production promoted by PMeCD-activated porphyrin photosensitization.

Moreover, the cell viability in the presence of prodrug and targeting agent was evaluated, showing that no obvious dose-dependent cytotoxicity was found for TPP-CA4 alone but the cytotoxicity apparently increased for the TPP-CA4⊂HA-

https://doi.org/10.1021/acs.jmedchem.2c00105
J. Med. Chem. 2022, 65, 6764−6774

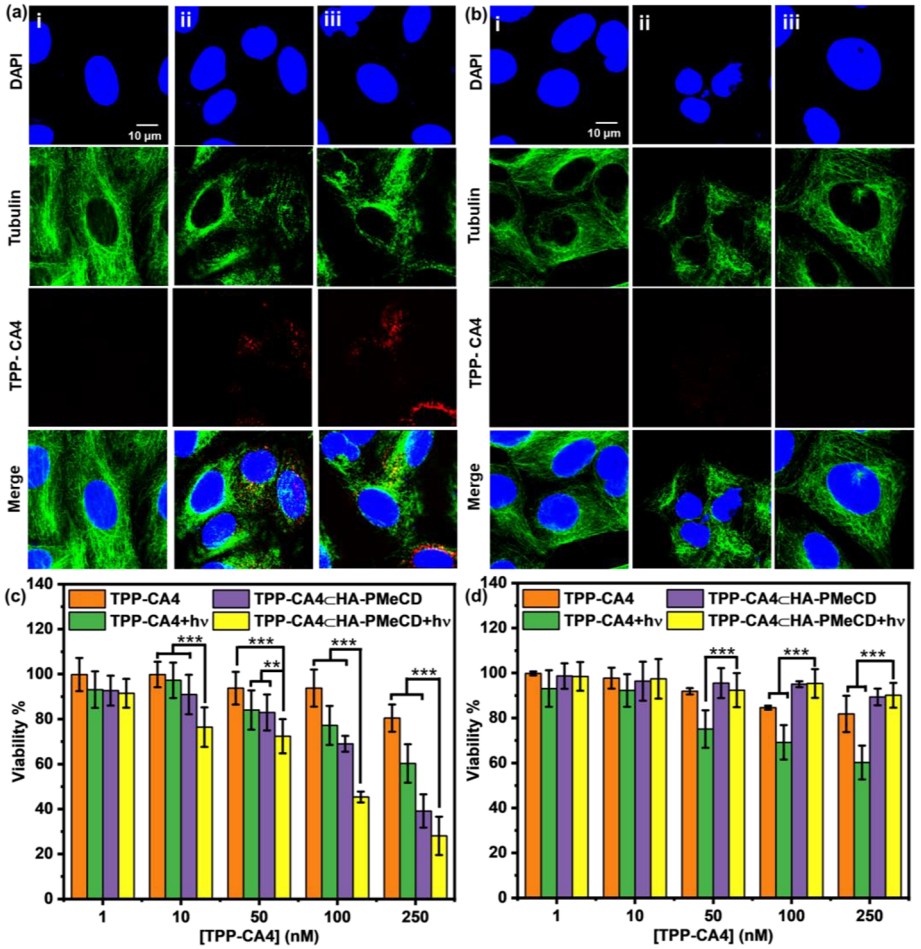

Figure 4. Confocal fluorescence images of (a) A549 and (b) 293T cells incubated with different samples followed by 650 nm light irradiation for 5 min: (i) blank control, (ii) TPP-CA4, (iii) TPP-CA4⊂HA-PMeCD assembly ([TPP-CA4] = 20 nM and [HA-PMeCD] = 40 nM). 4′,6-Diamidino-2-phenylindole (DAPI, blue) and tubulin tracker (green) were used to stain nucleus and cytoskeleton, respectively. The fluorescence of TPP-CA4 is red. The scale bar is 10 μm. Cell viability of (c) A549 and (d) 293T cells after incubation with TPP-CA4 and TPP-CA4⊂HA-PMeCD assembly for 12 h with and without light irradiation at 650 nm for 5 min at different concentrations. Statistically significant differences are indicated with asterisks ((***) $p < 0.001$, (**) $p < 0.01$, (*) $p < 0.05$), and all data were expressed as the mean ± standard error of the mean.

PMeCD assembly when exposed to light irradiation in the A549 cells (Figure 4c). Taking the concentration of TPP-CA4 at 100 nM as an example, no deleterious effect was observed without light irradiation and over 77.2% of cells remained alive after treatment with free TPP-CA4 under light irradiation. However, the cellular viability sharply declined under light irradiation after co-incubation with TPP-CA4 and HA-PMeCD for 12 h (45.4%). Comparatively, lacking the overexpressed HA-receptor on the cell surface, only low toxicity was found in the 293T cells under the same experimental condition (Figure 4d). The cytotoxicity effect could be directly distinguished by counting the number of living cells in the same wells after incubating with calcein-AM, a cell-permeant dye to selectively stain living cells. The number of living cells treated by TPP-CA4 in one-half well sharply decreased upon exposure to light irradiation, which resembled the phenomenon in the other half well without irradiation (Figure S20, Supporting Information). Also, similar observations with less living cells could be found with the assistance of HA-PMeCD. These results contribute to the co-release of $^1O_2$ and CA4 because the former with shorter lifetime could kill the cells only in the irradiated part but the latter could spread into the surrounding dark part. Due to the bystander effect, the released drug could diffuse in the whole well and then kill the neighboring cells even when one-half well was covered without light irradiation.

Fluorescence Imaging and Tumor-Growth Inhibition in Vivo. Considering the MT disruption and photodynamic properties of TPP-CA4⊂HA-PMeCD assembly at the cellular level, we were curious to know whether such complexation-boosted porphyrin photosensitization could be utilized to achieve targeted cancer theranostics in the animal mode. Therefore, the tumor-burdened mouse modes were established to evaluate the therapeutic outcomes. On account of the relatively low water-solubility of the resultant assembly, intratumoral injection was directly used to avoid the undesired vascular blockage in the treatment groups. The weight gain of mice was basically the same in all experimental groups, indicative that no systemic toxicity could be found in such light-activatable supramolecular prodrug delivery systems (Figure 5a). Moreover, the tumor growth rates became much slower over the entire experimental period when the mice were co-treated with TPP-CA4 and HA-PMeCD conjugate. The marginally acceptable treatment effect shown in the groups of TPP-CA4, TPP-CA4⊂PMeCD complex, and TPP-CA4⊂HA-PMeCD assembly is probably due to the instability of TPP-CA4 itself over a long period of time, which

https://doi.org/10.1021/acs.jmedchem.2c00105
J. Med. Chem. 2022, 65, 6764−6774

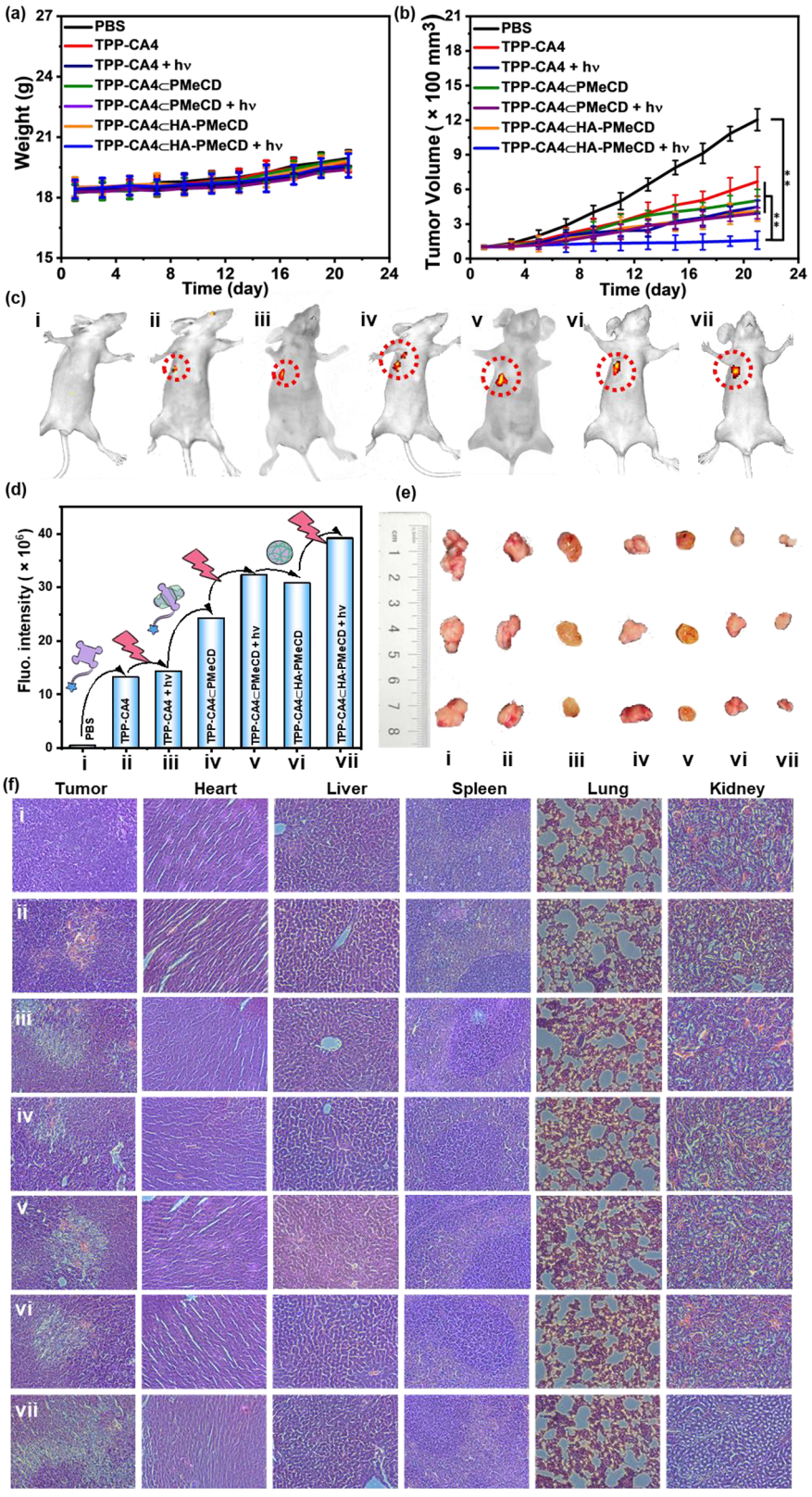

Figure 5. (a) Body weights of the mice in different groups after treatment at different time intervals. (b) Time-dependent tumor sizes from different groups of mice with different treatments over a period of 20 d. (c) In vivo fluorescence images of mice with different treatments after 7 d. (d) Fluorescence intensity of the in vivo fluorescence images of mice with different treatments. (e) Representative photographs of tumor at the end of the in vivo anticancer experiments (i, PBS; ii, TPP-CA4; iii, TPP-CA4 + *hν*; iv, TPP-CA4⊂PMeCD complex; v, TPP-CA4⊂PMeCD complex + *hν*; vi, TPP-CA4⊂HA-PMeCD assembly; and vii, TPP-CA4⊂HA-PMeCD assembly + *hν*). The Student's *t* test was used for statistical analysis (*p < 0.05, **p < 0.01, ***p < 0.001), and all data were expressed as the mean ± standard error of the mean. (f) H&E staining of tumor tissues (magnification 100×) from different samples of euthanized mice.

https://doi.org/10.1021/acs.jmedchem.2c00105
J. Med. Chem. 2022, 65, 6764−6774

could nonspecifically trigger the drug release process without exposure to light irradiation. In addition, lacking the HA chain as the targeted agent, only a moderate therapeutic effect was observed in the groups of TPP-CA4 + $h\nu$ and TPP-CA4⊂PMeCD complex + $h\nu$. Remarkably, benefiting from the targeted chemo- and photodynamic therapeutics, the tumor growth was completely inhibited under light irradiation (Figure 5b). Meanwhile, the complexation with HA-PMeCD could give rise to the selective in vivo fluorescence imaging behaviors; that is, only weak fluorescence could be detected when TPP-CA4 alone was injected, while strong fluorescence was observed in the presence of PMeCD under the same experimental condition (Figure 5c). These in vivo imaging observations are consistent with the quantitative data in Figure 5d. The relative tumor volumes were also compared after the mice were sacrificed, and as expected, the implementation of combinational therapy gave the best tumor ablation results among all the examined groups (Figure 5e). Accordingly, the histological observation of the hematoxylin and eosin (H&E) staining of main organs further substantiates that no significant lesions could be found in the normal organs of the mice after injecting the TPP-CA4⊂HA-PMeCD assembly, again corroborating the high biosafety and biocompatibility of the resultant supramolecular nanomedicine (Figure 5f). Overall, the in vivo animal experiments demonstrate that the tumor growth could be largely reversed and the tumor ablation could be efficiently achieved by combinational therapeutic methods of complexation-enhanced porphyrin photosensitization and light-activated drug release.

CONCLUSIONS

The porphyrin-based prodrug TPP-CA4 has been conveniently synthesized, and its corresponding nanoformulation has been fabricated by the strong host−guest complexation with HA-PMeCD. The noncovalent coating of TPP-CA4 with HA-PMeCD dramatically increased the $^1O_2$ production efficiency nearly 60-fold higher than that of the pristine prodrug, which could eventually promote the self-photocleavage of aminoacrylate linker and the drug release. As comprehensively investigated by both the cellular and animal experiments, the porphyrin core with the host−guest-binding-enhanced fluorescence emission can be utilized as a targeted cell/tissue-imaging agent and more significantly, the obtained binary TPP-CA4⊂HA-PMeCD assembly can seriously cause the destruction of MT backbones and efficiently suppress the tumor growth arising from the combinational therapies. Therefore, it can be anticipated that the development of supramolecular prodrug delivery systems with improved photophysical properties and stimuli-responsive characteristics will greatly enrich the research scope of modern nanomedicines and bring about more appealing theranostics strategies against many refractory diseases.

EXPERIMENTAL SECTION

Materials. All chemicals were commercially available reagent grade and used without further purification unless otherwise noted. The purity of TPP-CA4 was determined to be >95% by a combination of ^1H, ^{13}C NMR, HRMS, and HPLC analyses. HA-PMeCD and the precursor compound L-CA4 were synthesized according to the reported literature.[42,46] After the calculation of integral area in the ^1H spectrum, the modification degree of PMeCD units on the chain of HA is ∼14.3%.

Instruments. NMR spectra were recorded on a Bruker 400 MHz instrument, and chemical shifts were recorded in parts per million (ppm). High resolution mass (HRMS) spectra were performed on Q-TOF LC−MS with an ESI mode. TEM images were acquired by a high-resolution transmission electron microscope (Philips Tecnai G2 20S-TWIN microscope) operating at an accelerating voltage of 200 keV. The samples were prepared by placing a drop of solution onto a carbon-coated copper grid and air-dried. Transmission spectra were recorded on a Shimadzu UV-3600 spectrophotometer in a quartz cell (light path 10 mm) at 37 °C with a PTC-348WI temperature controller. Dynamic light scattering (DLS) was recorded on BI-200SM (Brookhaven Company) at 37 °C.

Chemical Synthesis of TPP-CA4. The synthetic route is shown in Scheme S1. The reaction mixture of L-CA4 (0.10 mmol, 48.4 mg), TPP-COOH (0.08 mmol, 52.7 mg), and TFA (20 μL) was dissolved in anhydrous DCM (20 mL) and stirred at room temperature for 2 h. Then, the solvent was removed under reduced pressure. The residue was dissolved in methanol, and then it was purified by HPLC. The corresponding compound TPP-CA4 was a red solid (24.75 mg, yield 25%). ^1H NMR (400 MHz, $CDCl_3$) δ 8.86 (s, 6H), 8.79 (m, 2H), 8.44 (d, J = 7.8 Hz, 2H), 8.32 (d, J = 8.2 Hz, 2H), 8.22 (d, J = 7.2 Hz, 6H), 7.79−7.74 (m, 9H), 7.57 (d, J = 12.2 Hz, 1H), 7.08 (d, J = 9.4 Hz, 2H), 6.83 (d, J = 8.5 Hz, 1H), 6.52 (s, 2H), 6.43 (d, J = 14.2 Hz, 2H), 4.89 (d, J = 12.9 Hz, 1H), 4.41 (d, J = 6.5 Hz, 2H), 3.36−3.78 (m, 6H), 3.71 (s, 8H), 3.14 (s, 2H), 2.21 (s, 1H), 2.03 (d, J = 14.3 Hz, 2H), 1.68 (s, 2H), −2.79 (s, 2H). ^{13}C NMR (100 MHz, $CDCl_3$) δ 162.8, 153.2, 151.9, 150.0, 141.0, 139.2, 136.1, 131.6, 128.0, 126.9, 126.8, 125.7, 122.9, 119.4, 110.8, 108.2, 104.9, 82.0, 59.9, 55.0, 50.2, 34.6, 30.7, 28.7, 21.7, 15.8. HRMS (QFT-ESI) m/z for $C_{72}H_{62}N_5O_8^+$ calcd $[M + H]^+$, 1124.4520; found, 1124.4562.

Preparation Procedure of Nanoparticle. First, the stock solution of HA-PMeCD (2 mM in PBS) and TPP-CA4 (1 mM in 1% DMSO or 10% DMSO in PBS) was prepared. Then, the same volumes of HA-PMeCD and TPP-CA4 solution were taken in each experiment. The mixed solution was sonicated for 15 min to obtain a uniform dispersion of nanoparticles and stored at 4 °C. Given the extraordinarily high binding strength between PMeCD and TPP in the formation of binary nanoparticles, the content of each component was simply used as their initial concentrations. The concentration of HA-PMeCD was calculated based on the PMeCD units.

Cell Viability Assay. To investigate the toxicity of TPP-CA4 and TPP-CA4⊂HA-PMeCD and them under light to the A549 lung tumor cells, the cells were cultured in 96-well plates in F12 medium containing 10% FBS for 24 h, and then the corresponding samples were added into the wells. The cells were further cultured for 12 h, and half of the cells were irradiated with 650 nm LED light. The cell growth was examined using the CCK-8 assay kit (Dojindo, Japan) in 10 min.

Inhibition Experiments of Tumor Growth. Four-week-old female BALB/c nude mice (n = 30, Weitonglihua, China) received 10^7/mL A549 cells in PBS (100 μL) into the right armpit by subcutaneous injection. After 14 days after tumor implantation, the mice were randomly divided into five groups (six mice per group). On the second day after the drug was injected, a 660 nm laser was used to irradiate the tumor site for 3 min. After 9 days of treatment, the mice were anaesthetized. The tumor volumes (V) were measured using a vernier caliper every 2 days and calculated using the following equation: $V = 0.5 \times (\text{tumor length}) \times (\text{tumor width})^2$. The relative tumor volumes were calculated as V/V_0 (V_0 is the tumor volume when the drug injection begins). The tissues of tumors and organs were stained with H&E and observed by a fluorescence microscope (DM3000, Leica, Germany). All experimental procedures were approved and in accordance with China's National Code of Animal Care for Scientific Experimentation. The experiments were also assessed by the Animal Experimentation Ethics Committee of Nankai University, and the assigned approval number is 2021-SYDELL-000448.

Computational Methods. Geometry optimization and frequency analysis were performed using Grimme's extended tight-binding model (GFN2-xTB)[50] by Gaussian 16 external program gau_xtb. The

https://doi.org/10.1021/acs.jmedchem.2c00105
J. Med. Chem. 2022, 65, 6764−6774

single-point calculations were further improved by using the B3LYP functional[51−53] and def2-SVP[54] basis set with SMD model (10% DMSO/water as solvent), at the same time using Grimme's DFT-D3 dispersion corrections[55] with Becke−Johnson finite-damping (DFT-D3(BJ)).[56] The visual molecular orbital diagram is made with GaussView 6.0 (isovalue = 0.02).

■ ASSOCIATED CONTENT

Supporting Information

The Supporting Information is available free of charge at https://pubs.acs.org/doi/10.1021/acs.jmedchem.2c00105.

Compound characterization, Job's plot, photoluminescence spectra, irradiation-time-dependent changes of the compounds in ^{1}H NMR and ^{13}C NMR spectra, photostability of compounds, HPLC retention times and the LC−MS spectrum of the corresponding peaks, theoretical calculation, and confocal fluorescence images (PDF)

Molecular formula string (CSV)

■ AUTHOR INFORMATION

Corresponding Authors

Ying-Ming Zhang − *College of Chemistry, State Key Laboratory of Elemento-Organic Chemistry, Nankai University, Tianjin 300071, China*; Email: ymzhang@nankai.edu.cn

Yu Liu − *College of Chemistry, State Key Laboratory of Elemento-Organic Chemistry, Nankai University, Tianjin 300071, China*; orcid.org/0000-0001-8723-1896; Email: yuliu@nankai.edu.cn

Authors

Mian Tang − *College of Chemistry, State Key Laboratory of Elemento-Organic Chemistry, Nankai University, Tianjin 300071, China*

Yanqiu Song − *Key Laboratory of Functional Polymer Materials, Ministry of Education, State Key Laboratory of Medicinal Chemical Biology, Institute of Polymer Chemistry, College of Chemistry, Nankai University, Tianjin 300071, China*

Yi-Lin Lu − *College of Chemistry, State Key Laboratory of Elemento-Organic Chemistry, Nankai University, Tianjin 300071, China*

Zhilin Yu − *Key Laboratory of Functional Polymer Materials, Ministry of Education, State Key Laboratory of Medicinal Chemical Biology, Institute of Polymer Chemistry, College of Chemistry, Nankai University, Tianjin 300071, China*; orcid.org/0000-0002-7116-3304

Xiufang Xu − *College of Chemistry, State Key Laboratory of Elemento-Organic Chemistry, Nankai University, Tianjin 300071, China*; orcid.org/0000-0002-3510-3267

Complete contact information is available at: https://pubs.acs.org/10.1021/acs.jmedchem.2c00105

Notes

The authors declare no competing financial interest.

■ ACKNOWLEDGMENTS

We thank Yifu Chen at Tianjin University for the preparation of Figure 3a and Figure 3b. This work was financially supported by the National Natural Science Foundation of China (Grants 21871154, 22171148, 22131008, and 21873051), Natural Science Foundation of Tianjin (Grant 21JCZDJC00310), and the Fundamental Research Funds for the Central Universities, Nankai University.

■ ABBREVIATIONS USED

CA4, combretastatin A-4; HA-PMeCD, permethyl-β-cyclodextrin-grafted hyaluronic acid; TPP-CA4, 5-(4-carboxyphenyl)-10,15,20-triphenylporphyrin modified by combretastatin A-4

■ REFERENCES

(1) Sun, C.; Wang, Z.; Yang, K.; Yue, L.; Cheng, Q.; Ma, Y.-L.; Lu, S.; Chen, G.; Wang, R. Polyamine-Responsive Morphological Transformation of a Supramolecular Peptide for Specific Drug Accumulation and Retention in Cancer Cells. *Small* **2021**, *17*, 2101139.

(2) Webber, M. J.; Langer, R. Drug Delivery by Supramolecular Design. *Chem. Soc. Rev.* **2017**, *46*, 6600−6620.

(3) Guan, X.; Chen, Y.; Wu, X.; Li, P.; Liu, Y. Enzyme-Responsive Sulfatocyclodextrin/Prodrug Supramolecular Assembly for Controlled Release of Anti-Cancer Drug Chlorambucil. *Chem. Commun.* **2019**, *55*, 953−956.

(4) Hu, B.; Song, N.; Cao, Y.; Li, M.; Liu, X.; Zhou, Z.; Shi, L.; Yu, Z. Noncanonical Amino Acids for Hypoxia-Responsive Peptide Self-Assembly and Fluorescence. *J. Am. Chem. Soc.* **2021**, *143*, 13854−13864.

(5) Cheetham, A. G.; Chakroun, R. W.; Ma, W.; Cui, H. Self-assembling Prodrugs. *Chem. Soc. Rev.* **2017**, *46*, 6638−6663.

(6) Wu, X.; Gao, L.; Hu, X.-Y.; Wang, L. Supramolecular Drug Delivery Systems Based on Water-Soluble Pillar[n]arenes. *Chem. Rec.* **2016**, *16*, 1216−1227.

(7) Xing, P.; Zhao, Y. Supramolecular Vesicles for Stimulus-Responsive Drug Delivery. *Small Methods* **2018**, *2*, 1700364.

(8) Su, H.; Zhang, P.; Cheetham, A. G.; Koo, J. M.; Lin, R.; Masood, A.; Schiapparelli, P.; Quinones-Hinojosa, A.; Cui, H. Supramolecular Crafting of Self-Assembling Camptothecin Prodrugs with Enhanced Efficacy Against Primary Cancer Cells. *Theranostics* **2016**, *6*, 1065−1074.

(9) Cheng, H.-B.; Zhang, Y.-M.; Liu, Y.; Yoon, J. Turn-On Supramolecular Host-Guest Nanosystems as Theranostics for Cancer. *Chem.* **2019**, *5*, 553−574.

(10) Tang, M.; Liu, Y.-H.; Xu, X.-M.; Zhang, Y.-M.; Liu, Y. Dual-responsive drug release and fluorescence imaging based on disulfide-pillar[4]arene aggregate in cancer cells. *Bioorg. Med. Chem.* **2022**, *57*, 116649.

(11) Geng, W.-C.; Sessler, J. L.; Guo, D.-S. Supramolecular Prodrugs Based on Host-Guest Interactions. *Chem. Soc. Rev.* **2020**, *49*, 2303−2315.

(12) Zhang, Y.-M.; Xu, X.; Yu, Q.; Liu, Y.-H.; Zhang, Y.-H.; Chen, L.-X.; Liu, Y. Reversing the Cytotoxicity of Bile Acids by Supramolecular Encapsulation. *J. Med. Chem.* **2017**, *60*, 3266−3274.

(13) Deng, Y.; Wang, Y.; Jia, F.; Liu, W.; Zhou, D.; Jin, Q.; Ji, J. Tailoring Supramolecular Prodrug Nanoassemblies for Reactive Nitrogen Species-Potentiated Chemotherapy of Liver Cancer. *ACS Nano* **2021**, *15*, 8663−8675.

(14) Chen, H.; Zeng, X.; Tham, H. P.; Phua, S. Z. F.; Cheng, W.; Zeng, W.; Shi, H.; Mei, L.; Zhao, Y. NIR-Light-Activated Combination Therapy with a Precise Ratio of Photosensitizer and Prodrug Using a Host-Guest Strategy. *Angew. Chem., Int. Ed.* **2019**, *58*, 7641−7646.

(15) Deng, X.; Shao, Z.; Zhao, Y. Solutions to the Drawbacks of Photothermal and Photodynamic Cancer Therapy. *Adv. Sci.* **2021**, *8*, 2002504.

(16) Feng, G.; Zhang, G.-Q.; Ding, D. Design of Superior Phototheranostic Agents Guided by Jablonski Diagrams. *Chem. Soc. Rev.* **2020**, *49*, 8179−8234.

(17) Luby, B. M.; Walsh, C. D.; Zheng, G. Advanced Photosensitizer Activation Strategies for Smarter Photodynamic Therapy Beacons. *Angew. Chem., Int. Ed.* **2019**, *58*, 2558−2569.

(18) Zhang, W.; Ji, T.; Li, Y.; Zheng, Y.; Mehta, M.; Zhao, C.; Liu, A.; Kohane, D. S. Light-Triggered Release of Conventional Local Anesthetics from a Macromolecular Prodrug for On-demand Local Anesthesia. *Nat. Commun.* **2020**, *11*, 2323.
(19) Zhou, S.; Hu, X.; Xia, R.; Liu, S.; Pei, Q.; Chen, G.; Xie, Z.; Jing, X. A Paclitaxel Prodrug Activatable by Irradiation in a Hypoxic Microenvironment. *Angew. Chem., Int. Ed.* **2020**, *59*, 23198−23205.
(20) Liu, L.-H.; Qiu, W.-X.; Li, B.; Zhang, C.; Sun, L.-F.; Wan, S.-S.; Rong, L.; Zhang, X.-Z. A Red Light Activatable Multifunctional Prodrug for Image-Guided Photodynamic Therapy and Cascaded Chemotherapy. *Adv. Funct. Mater.* **2016**, *26*, 6257−6269.
(21) Yu, Q.; Zhang, Y.-M.; Liu, Y.-H.; Liu, Y. Magnetic Supramolecular Nanofibers of Gold Nanorods for Photothermal Therapy. *Adv. Therap.* **2019**, *2*, 1800137.
(22) Cheng, H.-B.; Cui, Y.; Wang, R.; Kwon, N.; Yoon, J. The Development of Light-Responsive, Organic Dye Based, Supramolecular Nanosystems for Enhanced Anticancer Therapy. *Coord. Chem. Rev.* **2019**, *392*, 237−254.
(23) Li, X.; Park, E. Y.; Kang, Y.; Kwon, N.; Yang, M.; Lee, S.; Kim, W. J.; Kim, C.; Yoon, J. Supramolecular Phthalocyanine Assemblies for Improved Photoacoustic Imaging and Photothermal Therapy. *Angew. Chem., Int. Ed.* **2020**, *59*, 8630−8634.
(24) Sun, F.; Zhu, Q.; Li, T.; Saeed, M.; Xu, Z.; Zhong, F.; Song, R.; Huai, M.; Zheng, M.; Xie, C.; Xu, L.; Yu, H. Regulating Glucose Metabolism with Prodrug Nanoparticles for Promoting Photoimmunotherapy of Pancreatic Cancer. *Adv. Sci.* **2021**, *8*, 2002746.
(25) Yang, K.; Yu, G.; Yang, Z.; Yue, L.; Zhang, X.; Sun, C.; Wei, J.; Rao, L.; Chen, X.; Wang, R. Supramolecular Polymerization-Induced Nanoassemblies for Self-Augmented Cascade Chemotherapy and Chemodynamic Therapy of Tumor. *Angew. Chem., Int. Ed.* **2021**, *60*, 17570−17578.
(26) Olesen, M. T. J.; Walther, R.; Poier, P. P.; Dagnaes-hansen, F.; Zelikin, A. N. Molecular, Macromolecular, and Supramolecular Glucuronide Prodrugs: Lead Identified for Anticancer Prodrug Monotherapy. *Angew. Chem., Int. Ed.* **2020**, *59*, 7390−7396.
(27) Feng, H.-T.; Li, Y.; Duan, X.; Wang, X.; Qi, C.; Lam, J. W. Y.; Ding, D.; Tang, B. Z. Substitution Activated Precise Phototheranostics through Supramolecular Assembly of AIEgen and Calixarene. *J. Am. Chem. Soc.* **2020**, *142*, 15966−15974.
(28) Hu, D.; Deng, Y.; Jia, F.; Jin, Q.; Ji, J. Surface Charge Switchable Supramolecular Nanocarriers for Nitric Oxide Synergistic Photodynamic Eradication of Biofilms. *ACS Nano* **2020**, *14*, 347−359.
(29) Wang, D.; Tang, B. Z. Aggregation-induced Emission Luminogens for Activity-based Sensing. *Acc. Chem. Res.* **2019**, *52*, 2559−2570.
(30) Luby, B. M.; Charron, D. M.; MacLaughlin, C. M.; Zheng, G. Activatable Fluorescence: From Small Molecule to Nanoparticle. *Adv. Drug Delivery Rev.* **2017**, *113*, 97−121.
(31) Li, X.; Kim, C.-Y.; Lee, S.; Lee, D.; Chung, H. M.; Kim, G.; Heo, S. H.; Kim, C.; Hong, K.-S.; Yoon, J. Nanostructured Phthalocyanine Assemblies with Protein-Driven Switchable Photoactivities for Biophotonic Imaging and Therapy. *J. Am. Chem. Soc.* **2017**, *139*, 10880−10886.
(32) Zhang, Y.; Tao, H.; Li, Q.; Sheng, W.; Xu, Y.; Hao, E.; Chen, M.; Liu, Z.; Feng, L. Surfactant-stripped J-aggregates of azaBODIPY Derivatives: All-in-one Phototheranostics in the Second Near Infrared Window. *J. Controlled Release* **2020**, *326*, 256−264.
(33) Ikeda, A.; Satake, S.; Mae, T.; Ueda, M.; Sugikawa, K.; Shigeto, H.; Funabashi, H.; Kuroda, A. Photodynamic Activities of Porphyrin Derivative-Cyclodextrin Complexes by Photoirradiation. *ACS Med. Chem. Lett.* **2017**, *8*, 555−559.
(34) Wu, X.; Sun, X.; Guo, Z.; Tang, J.; Shen, Y.; James, T. D.; Tian, H.; Zhu, W. In vivo And in Situ Tracking Cancer Chemotherapy by Highly Photostable NIR Fluorescent Theranostic Prodrug. *J. Am. Chem. Soc.* **2014**, *136*, 3579−3588.
(35) Ma, Z.-l.; Yan, X.-j.; Zhao, L.; Zhou, J.-j.; Pang, W.; Kai, Z.-p.; Wu, F.-h. Combretastatin A-4 and Derivatives: Potential Fungicides Targeting Fungal Tubulin. *J. Agric. Food Chem.* **2016**, *64*, 746−751.
(36) Gerova, M. S.; Stateva, S. R.; Radonova, E. M.; Kalenderska, R. B.; Rusew, R. I.; Nikolova, R. P.; Chanev, C. D.; Shivachev, B. L.; Apostolova, M. D.; Petrov, O. I. Combretastatin A-4 analogues with benzoxazolone scaffold: Synthesis, structure and biological activity. *Eur. J. Med. Chem.* **2016**, *120*, 121−133.
(37) Tian, H.; He, Z.; Sun, C.; Yang, C.; Zhao, P.; Liu, L.; Leong, K. W.; Mao, H. Q.; Liu, Z.; Chen, Y. Uniform Core-Shell Nanoparticles with Thiolated Hyaluronic Acid Coating to Enhance Oral Delivery of Insulin. *Adv. Healthcare Mater.* **2018**, *7*, 1800285.
(38) Lei, C.; Liu, X.-R.; Chen, Q.-B.; Li, Y.; Zhou, J.-L.; Zhou, L.-Y.; Zou, T. Hyaluronic Acid and Albumin Based Nanoparticles for Drug Delivery. *J. Controlled Release* **2021**, *331*, 416−433.
(39) Pulakkat, S.; Balaji, S. A.; Rangarajan, A.; Raichur, A. M. Surface Engineered Protein Nanoparticles with Hyaluronic Acid Based Multilayers for Targeted Delivery of Anticancer Agents. *ACS Appl. Mater. Interfaces* **2016**, *8*, 23437−23449.
(40) Kitagishi, H.; Chai, F.; Negi, S.; Sugiura, Y.; Kano, K. Supramolecular Intracellular Delivery of an Anionic Porphyrin by Octaarginine-Conjugated Per-O-methyl-β-cyclodextrin. *Chem. Commun.* **2015**, *51*, 2421−2424.
(41) Bonchio, M.; Carofiglio, T.; Carraro, M.; Fornasier, R.; Tonellato, U. Efficient Sensitized Photooxygenation in Water by a Porphyrin−Cyclodextrin Supramolecular Complex. *Org. Lett.* **2002**, *4*, 4635−4637.
(42) Rajora, M. A.; Lou, J. W. H.; Zheng, G. Efficient Sensitized Photooxygenation in Water by a Porphyrin−Cyclodextrin Supramolecular Complex. *Chem. Soc. Rev.* **2017**, *46*, 6433−6469.
(43) Bio, M.; Rajaputra, P.; Nkepang, G.; Awuah, S. G.; Hossion, A. M.; You, Y. Site-Specific and Far-Red-Light-Activatable Prodrug of Combretastatin A-4 Using Photo-Unclick Chemistry. *J. Med. Chem.* **2013**, *56*, 3936−3942.
(44) Bio, M.; Nkepang, G.; You, Y. Click and Photo-Unclick Chemistry of Aminoacrylate For Visible Light-Triggered Drug Release. *Chem. Commun.* **2012**, *48*, 6517−6519.
(45) Tham, H. P.; Xu, K.; Lim, W. Q.; Chen, H.; Zheng, M.; Thng, T. G. S.; Venkatraman, S. S.; Xu, C.; Zhao, Y. Microneedle-assisted Topical Delivery of Photodynamically Active Mesoporous Formulation for Combination Therapy of Deep-Seated Melanoma. *ACS Nano* **2018**, *12*, 11936−11948.
(46) Zhu, W.; Kang, M.; Wu, Q.; Zhang, Z.; Wu, Y.; Li, C.; Li, K.; Wang, L.; Wang, D.; Tang, B. Z. Zwitterionic AIEgens: Rational Molecular Design for NIR-II Fluorescence Imaging-Guided Synergistic Phototherapy. *Adv. Funct. Mater.* **2021**, *31*, 2007026.
(47) Yang, Y.; Zhang, Y.-M.; Chen, Y.; Chen, J.-T.; Liu, Y. Targeted Polysaccharide Nanoparticle for Adamplatin Prodrug Delivery. *J. Med. Chem.* **2013**, *56*, 9725−9736.
(48) Zhang, Y.-H.; Zhang, Y.-M.; Sheng, X.; Wang, J.; Liu, Y. Enzyme-Responsive Fluorescent Camptothecin Prodrug/Polysaccharide Supramolecular Assembly for Targeted Cellular Imaging and in Situ controlled Drug Release. *Chem. Commun.* **2020**, *56*, 1042−1045.
(49) El Kechai, N.; Mamelle, E.; Nguyen, Y.; Huang, N.; Nicolas, V.; Chaminade, P.; Yen-Nicolay, S.; Gueutin, C.; Granger, B.; Ferrary, E.; Agnely, F.; Bochot, A. Hyaluronic Acid Liposomal Gel Sustains Delivery of a Corticoid to the Inner Ear. *J. Controlled Release* **2016**, *226*, 248−257.
(50) Grimme, S.; Bannwarth, C.; Shushkov, P. A Robust and Accurate Tight-Binding Quantum Chemical Method for Structures, Vibrational Frequencies, and Noncovalent Interactions of Large Molecular Systems Parametrized for All spd-Block Elements (Z = 1−86). *J. Chem. Theory Comput.* **2017**, *13*, 1989−2009.
(51) Raghavachari, K. Perspective on "Density Functional Thermochemistry. III. The Role of Exact Exchange". *Theor. Chem. Acc.* **2000**, *103*, 361−363.
(52) Becke, A. D. A New Mixing of Hartree−Fock and Local Density-functional Theories. *J. Chem. Phys.* **1993**, *98*, 1372−1377.
(53) Lee, C.; Yang, W.; Parr, R. G. Development of the Colle-Salvetti Correlation-energy Formula into a Functional of the Electron Density. *Phys. Rev. B* **1988**, *37*, 785−789.

https://doi.org/10.1021/acs.jmedchem.2c00105
J. Med. Chem. 2022, 65, 6764−6774

(54) Schäfer, A.; Horn, H.; Ahlrichs, R. Fully Optimized Contracted Gaussian Basis Sets for Atoms Li to Kr. *J. Chem. Phys.* **1992**, *97*, 2571−2577.
(55) Grimme, S.; Antony, J.; Ehrlich, S.; Krieg, H. A Consistent and Accurate Ab Initio Parametrization of Density Functional Dispersion Correction (DFT-D) for the 94 Elements H-Pu. *J. Chem. Phys.* **2010**, *132*, 154104.
(56) Grimme, S.; Ehrlich, S.; Goerigk, L. Effect of the Damping Function in Dispersion Corrected Density Functional Theory. *J. Comput. Chem.* **2011**, *32*, 1456−1465.

https://doi.org/10.1021/acs.jmedchem.2c00105
J. Med. Chem. 2022, 65, 6764−6774